Progress In Electromagnetics Research C, Vol. 108, 1–12, 2021

Air-Gap Correction for High Power Microwave Measurements of Conductive Materials

John Lancaster[1, *], Daniel Chandler[1], Eun J. Moon[1], Ahmed Hassan[2], and Anthony Caruso[1]

Abstract—Measurements of the complex permittivity and permeability of solids at high electromagnetic field greater than 10 kV/m pose a significant challenge to RF connectors and input amplifiers of the measurement equipment. Specifically, difficulties arise in measuring materials with high imaginary permittivity or low impedance, which act as short circuits, either exceeding the measurement equipment damage threshold or that of the material under test, and/or inducing an unacceptable signal-to-noise in the collected data. In this work, we report the development of a new measurement technique where we introduce an outer air-gap between the material under test and the conductor of a coax airline. The introduced air-gap reduces the effective conductivity of the sample, mitigating damage to the materials under test and allowing for high power measurement. This study compares the ability of air-gap correction methods to recover the complex permittivity and permeability to within 10% of the value measured without an air-gap introduced.

1. INTRODUCTION

There has been a strong demand for the measurement of the electronic properties of materials at high field strengths for microwave frequencies. Such measurements are necessary for developing smart materials with the ability to tune their permittivity and/or permeability based on the level of incident field strength. Power dependent electronic properties of materials such as ferroelectric [1, 2], carbon allotropes [3, 4], and synergistic materials [5–8] have been extensively demonstrated, but require highly constrained testing topologies [1, 2] to measure permittivity alone and/or are incapable of testing materials with non-unity permeability [9]. These limitations on material test procedures, apparatus, or topology reduce the ability for direct comparison of the electromagnetic properties as a function of incident field strength. Interest in shielding effectiveness of the material [10] excludes waveguide based materials measurement techniques [11] due to the inability to resolve the electronic response of the material due to non-uniform field strength [12] of TE or TM propagation.

Measuring both the complex permittivity and permeability of conductive materials at high field strength has not been demonstrated under any reported testing topology. This deficiency is because materials with loss tangent, $\tan\delta > 0.05$, create a conductive path between the center and outer conductors of a coaxial air-line, creating a short circuit at high powers. The conductive path can alter the properties of the transmission line making the measurement erroneous, as well as damaging the Material Under Test (MUT), and possibly the measurement instrument. Shorting across the MUT is eliminated at the powers of interest (> 10 watts or 40 dBm) by introducing an outer air-gap between the MUT and the outer conductor of the coax airline. The introduction of the air-gap reduces the effective conduciveness and can be reversible, which will be discussed in greater detail in Section 2.

Received 26 November 2020, Accepted 28 December 2020, Scheduled 6 January 2021

* Corresponding author: John Lancaster (jl3y9@mail.umkc.edu).

[1] Department of Physics, University of Missouri, Kansas City, USA. [2] Department of Computer Science Electrical Engineering, University of Missouri, Kansas City, USA.

Retrieving the properties of the MUT after introducing the air-gap was investigated through volumetric based corrections and capacitive correction model. The volumetric corrections consist of two Effective Medium Approximations (EMA) (Bruggeman and Maxwell-Garnett) and a simple volume correction that accounts for the volume of material missing due to the introduced air-gap. The study considers either outer, Fig. 1(a), or inner air-gaps, Fig. 1(b), separately because introducing both inner and outer air-gaps will produce asymmetry in the location of the MUT in the coaxial airline, as shown in Fig. 1(c).

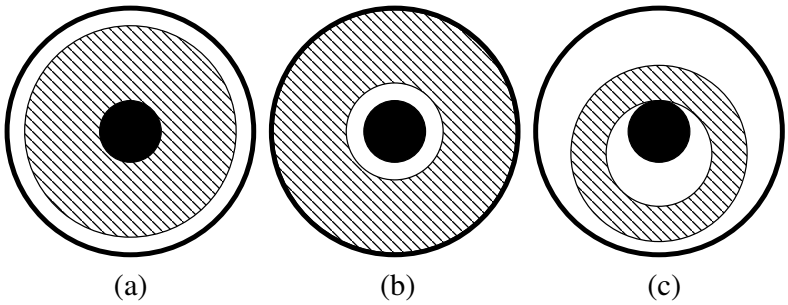

Figure 1. Diagram of MUT with (a) outer air-gap, (b) inner air-gap, and (c) inner and outer air-gap, demonstrating why both air-gaps are not considered.

In this paper, we present the dependency of measured complex permittivity and permeability, as a function of inner and outer air gap radii (four for each) for three MUTs (HDPE $\epsilon_r = 2.4$, $\tan\delta = 0.0005$, and $\mu_r = 1$, Macor $\epsilon_r = 5.4$, $\tan\delta = 0.0025$ [13], and $\mu = 1$, and Eccosorb MF-110 $\epsilon_r = 3.6$, $\tan\delta = 0.03$, and $\mu_r = 1.1$) across frequency range from 0.7 to 3 GHz. The low-loss materials were targeted to demonstrate the concept of retrieving accurate electronic properties of a MUT at high power below the conductivity threshold that will damage the material, with varied permittivity, loss tangent, and permeability. The study isolates the effect of real permittivity and inner and outer air-gap radius on the ability to recover the complex permittivity and permeability of unknown MUT.

2. THEORETICAL MODEL

A majority of broadband transmission line approaches to measuring complex permittivity and permeability are derived from of Nicolson and Ross [13] and Weir [14] for both time and frequency domain measurements of scattering parameters. The procedure to derive complex permittivity and permeability is performed by measuring the magnitude of reflections caused by impedance mismatches and varied electrical length of the transmission line due to the introduction of an MUT with known [15].

2.1. Algorithm

The algorithm used in this study to calculate the unknown complex permittivity and permeability of a MUT placed in a coaxial airline is similar to the algorithm introduced by Barry [16]. The characteristic impedance of the empty coax airline is given by $Z_0 = \sqrt{\mu_0/\epsilon_0}$, while the characteristic impedance for the loaded transmission line is changed to Z, where:

$$Z = Z_0\sqrt{\mu_r/\epsilon_r} \tag{1}$$

The propagation constant in the empty coax airline is given by $k_o = \omega\sqrt{\epsilon_0\mu_0}$, and the propagation constant of the MUT is changed to k, where:

$$k = k_0\sqrt{\epsilon_r\mu_r} \tag{2}$$

Z and k are both complex numbers that can be related to the complex permittivity ϵ_r and

permeability μ_r through the following equations:

$$\epsilon_r = \frac{k}{k_0}\left(\frac{1-R}{1+R}\right) \tag{3}$$

$$\mu_r = \frac{k}{k_0}\left(\frac{1+R}{1-R}\right). \tag{4}$$

Determination of k and R, where R is the reflectivity, from scattering parameters is given by the relationship of voltages and phase delay measured at each port of the VNA. The contribution from the MUT to the phase delay and reflection is determined through breaking up the coax airline into three sections, two of which are the properties of the empty coax airline (k_o and Z_o), and the center section with properties is determined by the MUT filled coax airline (k and Z). The k and Z from measured quantities S_{11} and S_{21} are given by

$$kt = \cos^{-1}\left(\frac{e^{-j4k_0l} + S_{12}^2 - S_{11}^2}{2e^{-j2k_0l}S_{12}}\right) \tag{5}$$

$$R = \frac{S_{11}}{(e^{-j2k_0L} - S_{12}e^{-jkt})}, \tag{6}$$

where t is the thickness of the MUT, and l is the length of the empty airline sections. The assumption for these calculations is that the MUT completely fills the coaxial airline and is homogeneous and isotropic.

The measured real permittivity for the MUT is shown in Figs. 2–4.

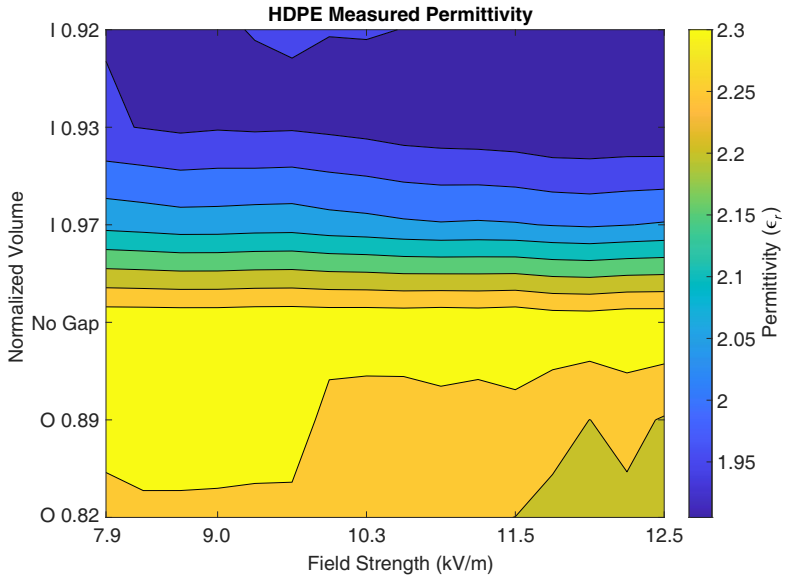

Figure 2. Measured permittivity at several field strengths for varied inner and outer air-gaps of HDPE. The upper half of the plot is for inner air-gaps, specified by "I 0.XX" followed by the normalized volume, and the outer gaps similarly labeled, "O 0.XX".

2.2. Time-Gate Filtering

Impedance matching of connectors and terminations across all frequencies of interest is improbable, which leads to additional origins for reflections from impedance mismatches. The reflections resulting from the impedance mismatches introduced by the MUT are repeatedly reflected from these additional interfaces resulting in repeated reflections that cause an oscillatory response in the frequency domain as well as significant noise to the measurement. The additional noise introduced by this process is mitigated by Fourier Transforming the frequency information from the VNA, placing a window at

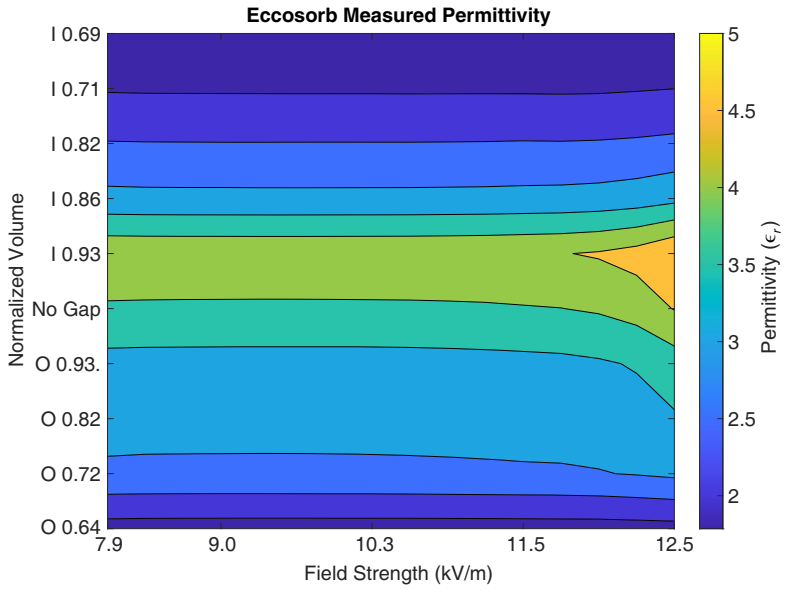

Figure 3. Measured permittivity at several field strengths for varied inner and outer air-gaps of Eccosorb. The upper half of the plot is for inner air-gaps, specified by "I 0.XX" followed by the normalized volume, and the outer gaps similarly labeled, "O 0.XX".

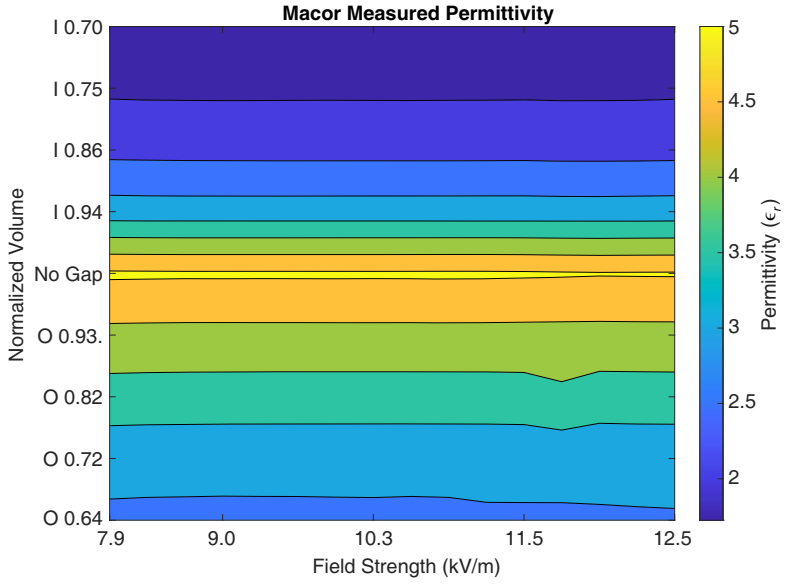

Figure 4. Measured permittivity at several field strengths for varied inner and outer air-gaps of Macor. The upper half of the plot is for inner air-gaps, specified by "I 0.XX" followed by the normalized volume, and the outer gaps similarly labeled, "O 0.XX".

a time associated with the electrical length of the transmission line which reduces the contribution from repeated reflections [17]. Time-Gate filtering for magnetic materials requires measurements of the MUT against a short standard, which was not considered for our study due to the complications of short standards that can withstand high power measurements, as short standards are low impedance and are not tolerant of the power levels needed, and the reflected power can be destructive to the VNA.

3. AIR-GAP CORRECTION METHODS

Variation from a completely filled coax airline can be mitigated by the use of air-gap correction methods. In this study air-gap correction is approached through two methods:

(i) Volumetric corrections of the permittivity and permeability which use the volume ratios of the MUT compared to that of the volume required to fill the coax airline.
   (a) Bruggeman EMA correction
   (b) Maxwell-Garnett EMA correction
   (c) Simple Volume correction — permittivity and permeability divided by the relative volume of the MUT as compared to volume without an air-gap.

(ii) A capacitive correction which uses each interface between the layers of material and air with the assumption that each layer behaves in a similar fashion to series capacitors (permittivity) [18] and/or inductors (permeability) [19].

One or the combination of correction mitigation methods will allow for determination of the complex permittivity and permeability of highly conductive MUT.

3.1. Volume Correction — Bruggeman EMA

Several methods have been developed to approximate properties of macroscopically inhomogeneous media in order to quantify the effective permittivity and conductivity resulting from a mixture of several materials. The Bruggeman EMA [20] considers that two isotropic materials with different permittivities (ϵ_s and ϵ_g sample and gap permittivities respectively) considered as spherical particles with volume fractions f_s and $f_g = 1 - f_s$ with the permittivity of the mixture given by ϵ_{BR}^{eff} will result in sample permittivity ϵ_s given by:

$$\epsilon_s = \frac{3\epsilon_B^{eff}}{f_g(\epsilon_g) + f_s(\epsilon_g)}\epsilon_{BR}^{eff} \tag{7}$$

3.2. Volume Correction — Maxwell-Garnett EMA

Maxwell-Garnett EMA [20] approximates the permittivity of an isotropic mixture ϵ_{MG}^{eff}, but through considering a media (ϵ_s used for comparison) and air inclusions with permittivity ϵ_g with the same volume ratios considered in the Bruggeman EMA, and results in the following inverse determination of an unknown ϵ_s given by:

$$\epsilon_s = \frac{(2 + f_s)\epsilon_{MG}^{eff} - 2f_g\epsilon_g}{(1 + 2f_s)\epsilon_g - f_g\epsilon_{MG}^{eff}}\epsilon_g \tag{8}$$

Considering the electrically small dimensions and cylindrical symmetry of the measurement the air-gap is isotropic.

3.3. Volume Correction

Both Maxwell-Garnett and Bruggeman EMA approaches converge to a simple ratio consisting of volume of the media, which is also greatly simplified in this study because the media of the air-gap has $\epsilon_r = 1$, and we consider the sample permittivity accounting for the volume of the MUT. Additionally this as a metric to determine how much of the difference in measurements is due simply to the reduction of the MUT volume.

3.4. Capacitive Air-Gap Correction

Assuming a homogenous transmission line the per unit length inductance and capacitance of a coaxial transmission line are given by:

$$L = \frac{1}{2\pi \ln(r_{out}/r_{in})} \tag{9}$$

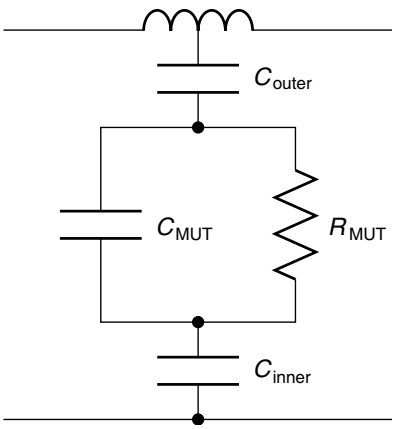

Figure 5. Transmission line model for a coaxial airline with outer and inner air-gaps with a Material Under Test (MUT), where C_{MUT} represents the real portion of permittivity and R_{MUT} represents the imaginary portion of permittivity of the MUT. The outer and inner air gaps, C_{outer} and C_{inner} are function of the size of the gap between the MUT and coaxial airline.

$$C = \frac{2\pi\epsilon_r^*}{\ln(r_{out}/r_{in})} \tag{10}$$

where r_{out}, r_{in}, and ϵ^* are the outer radius, inner radius, and complex permittivity of the homogenous line. Inner and outer air-gaps can be analyzed and modeled as series capacitance [19, 21] as shown in Fig. 5, which gives the effective capacitance of a transmission line with an air-gap as

$$C_{\mathit{eff}}^* = \frac{C_s^* C_g^*}{C_s^* + C_g^*}. \tag{11}$$

The above equation can be used to determine the effective permittivity ϵ_{eff} for the transmission line using Equations (9), (10) [24],

$$\epsilon_{\mathit{eff}}^* = \frac{\epsilon_s^* \epsilon_g^* L_c}{L_g \epsilon_g^* + L_s \epsilon_s^*} \tag{12}$$

where the inductances per unit are defined for the coaxial airline $L_c = \ln(r_{oc}/r_{ic})$, sample $L_s = \ln(r_{os}/r_{is})$, and gap $L_g = L_c - L_s$ for outer and inner air-gaps, respectively.

3.5. Air-Gap Concerns

Introducing air-gaps in high permittivity materials is expected [15, 22, 23] to have additional losses due to the appearance of higher order modes induced through the discontinuity between the MUT and the test fixture. Focusing on short MUT and looking for unexpected dips in S_{11} of higher frequency are known approaches for mitigating effects from higher order modes. The generation of higher order modes is not expected to have power dependency, but a possible frequency dependency. These tests were performed on electrically thin samples (2 mm thick) at low frequencies, and analysis is performed for each frequency in order to isolate power dependency for each MUT.

4. REDUCTION OF CONDUCTIVITY WITH AIR-GAPS

Introduction of an air-gap mitigates damage resulting from materials with high conductivity at high powers by creating additional series capacitance to the capacitance and resistance of the MUT effectively changes the transmission line properties, which is shown in Fig. 1. Analysis on the introduction of an air-gap to a coaxial transmission line has shown [24] reduced effective conductivity.

For the case of an air gap $\epsilon_{air} = 1$ allowing Eq. (12) to simplify to:

$$\epsilon_{\mathit{eff}}^* = \frac{\epsilon_s^* L_c}{L_g \epsilon_s^* + L_s} \tag{13}$$

for the case of an outer air-gap. Separating Eq. (13) into real and imaginary portions, the effective conductivity σ_{eff} is a function of the complex permittivity of the material $\epsilon_s^* = \epsilon_s' + i\epsilon_s''$ and the size of the air-gap, which is given by:

$$\tan\delta_{eff} = \frac{L_s \tan\delta_s}{\epsilon_s' L_g(1+\tan^2\delta_s) + L_s}. \tag{14}$$

where $\tan\delta_s = \sigma_s/(\omega\epsilon_0\epsilon_s)$ is the loss tangent of the MUT, and L_s and L_g are the inductances due to the sample and gap, respectively. Equation (14) is plotted in Fig. 6 for a 7 cm diameter coaxial airline at 2 GHz with a MUT permittivity $\epsilon_r = 10$. The ability to recover MUT conductivity σ_s from the measured conductivity depends on the sample conductivity, frequency tested, permittivity, and magnitude of the air-gap.

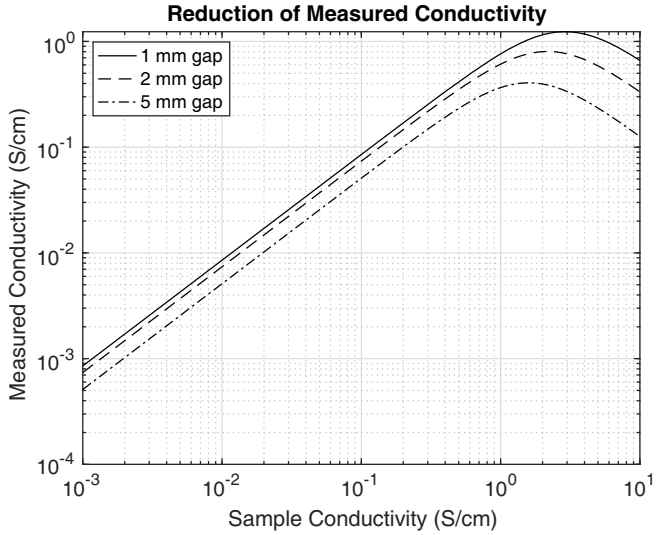

Figure 6. Plot demonstrating the reduced measured conductivity, and maximum acceptable conductivity that can accurately be measured in a 7 cm coaxial airline at 2 GHz with a MUT permittivity $\epsilon_r = 10$.

5. EXPERIMENT

The three different MUTs are characterized at low power, 0 dBm, using a precision coaxial airline (Maury Microwave) [25] with APC-7 connectors composed of an inner conductor diameter of 3-mm and an outer diameter of 7-mm. The coaxial airline varies from airlines for shielding measurements [10] having a reduced diameter that increases the maximum frequency and the field strength incident on the MUT. The APC-7 connectors are transitioned via SMA to the system components (Fig. 7). The coaxial airline is connected to a Rohde & Schwarz VZA24 vector network analyzer (VNA). High field strength measurements are made with incident power to the coax airline, swept from 20 to 50 dBm, using a Rohde & Schwarz BBA 150 amplifier from 0.7 to 3 GHz. Reference signal after the external amplifier is required by the VNA to account for phase and amplitude mismatches resulting from the amplifier. To address the problem of reference after the external amplifier, in addition to adding a reflect measurement from the coaxial airline, a directional coupler is input into external access ports of the VNA as illustrated in Fig. 7.

The four ports of the VNA are source (S), reference (R), reflection (A), and transmission (B). The scattering parameters used for materials measurement are:

$$S_{11} = A/R \tag{15}$$

$$S_{21} = B/R. \tag{16}$$

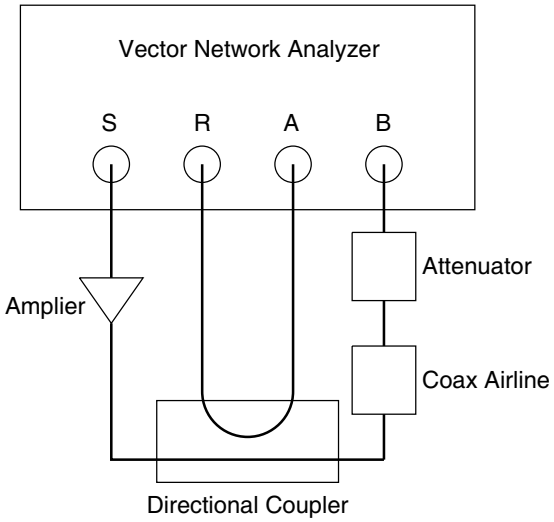

Figure 7. Block diagram of high power materials measurement system used for air-gap studies, where S = source, R = reference, A = reflection, and B = transmission measurements of the VNA.

Scattering parameters S_{11} and S_{21} are the only measurements made due to the directionality of the external amplifier [26, 27]. The incident power levels to the coax airline are confirmed with a Rohde & Schwarz NRP24 power meter in place of the coax airline. The amplitude and phase response of the amplifier, directional coupler, and attenuator are accounted for by the Short-Open-Load-Through (SOLT) calibration method, performed before all MUT tests.

The MUTs were prepared on a precision lathe to minimize the errors introduced due to unintentional air-gaps, alignment issues, and surface variations. Measurements are first made without a material placed in the coax airline. Empty measurements are used to eliminate power dependent properties of the coax airline and connectors, which are subsequently used to determine the electrical length of the airline for time gated algorithms [17]. The MUT is then placed in the coax airline to be measured, but its position within the cavity is unknown and needed to account for propagation through the airline. To remedy this the coax airline and SMA connectors are rotated 180° allowing the MUT to be electrically shifted to the center of the device. Combining two measurements to electrically shift the MUT to the center of the device is acceptable only when the MUT is homogeneous and isotropic [21].

In order to ensure that the values of the electronic properties are properly attributed to the varied incident field strength, and not the rise in temperature due to microwave absorption, the temperature is measured for all material measurements using an Omega OS36 non-contact infrared thermocouple. The temperature variations remained less than 2°C during the material measurement and should have limited effect, less than 10% MUT permittivity change on MUT for simple plastics [28] and perovskites [29]. The individual samples for the air-gap variations are then measured in the same manner for each MUT. The complex permittivity and permeability values are determined by the algorithms as outlined in Section 2.

6. RESULTS AND DISCUSSION

The introduction of an air gap reduces the measured permittivity of the MUT for all normalized material volumes, which is expected with the volume of the MUT replaced with the air $\epsilon_r \approx 1$. The error in measured permittivity is greater for inner air-gaps than for outer air gaps, and this response has been mentioned in literature [18, 19] and shown in Figs. 9–11 for HDPE, Macor, and Eccosorb respectively for measurements at 2 GHz. Eccosorb appears to have increased permittivity at power levels greater than 12 kV/m, and this response was recorded with each individual measurement of the Eccosorb samples, across all frequencies and has been determined to be a property of the material.

An example of the ability to recover the real permittivity measured for some algorithms considered

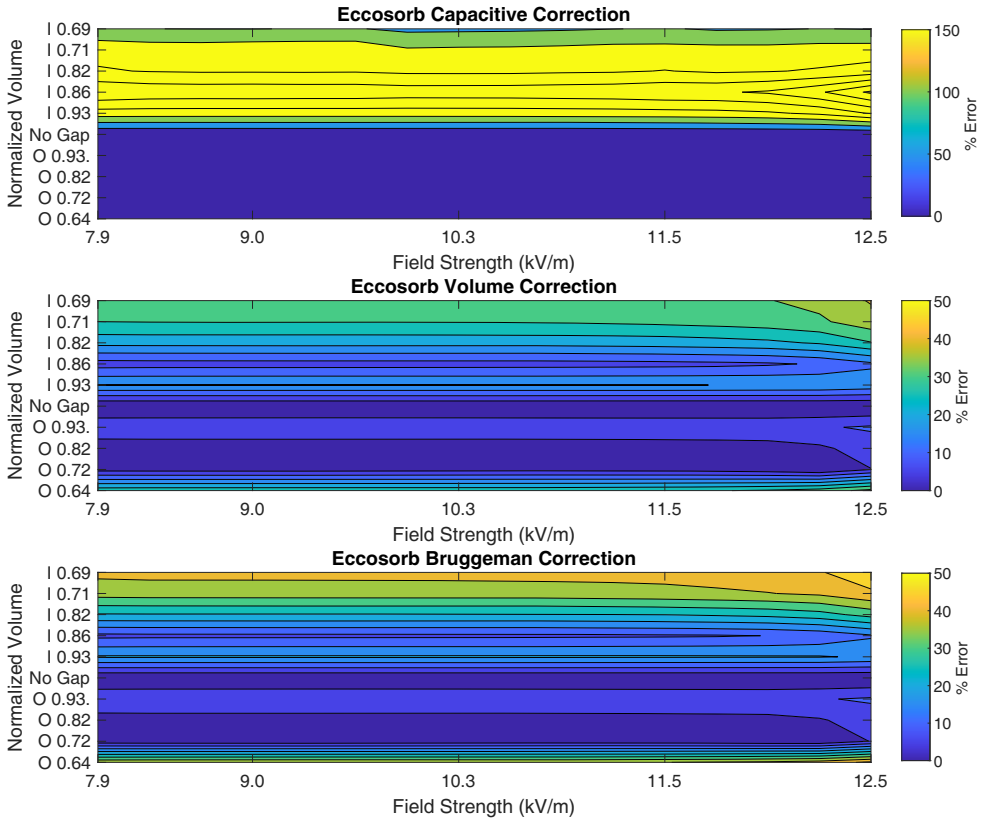

Figure 8. Percent error for measured permittivity of Eccosorb at several field strengths for varied inner and outer air-gaps. The upper half of the plot is for inner air-gaps, specified by "I 0.XX" followed by the normalized volume, and the outer gaps similarly labeled, "O 0.XX" for capacitive, volume and Bruggeman corrections.

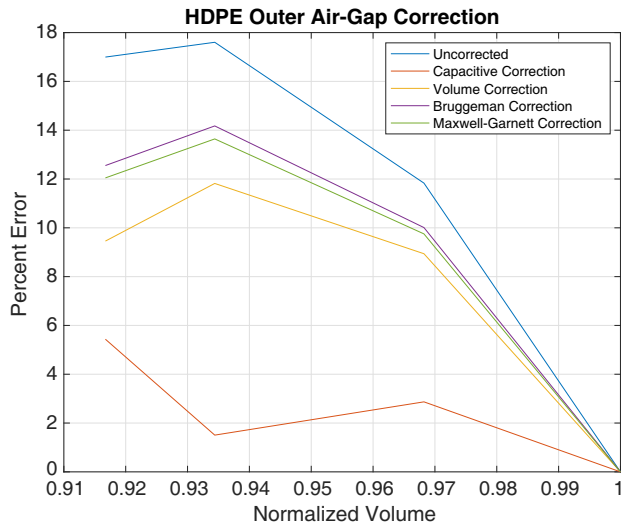

Figure 9. Percent error for outer air-gap correction methods for normalized volumes of HDPE.

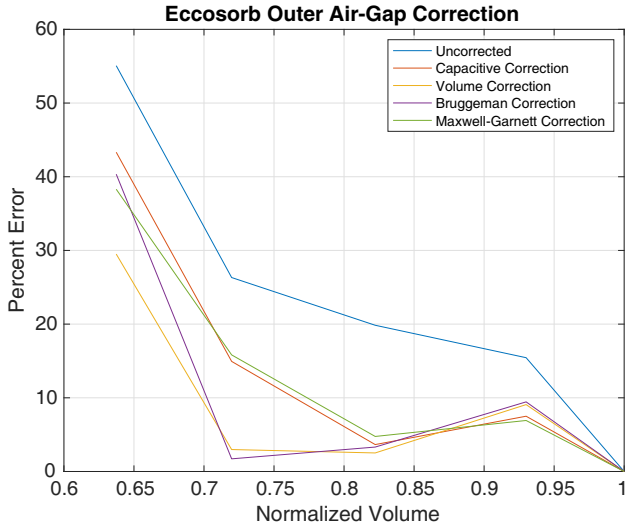

Figure 10. Percent error for outer air-gap correction methods for normalized volumes of Eccosorb.

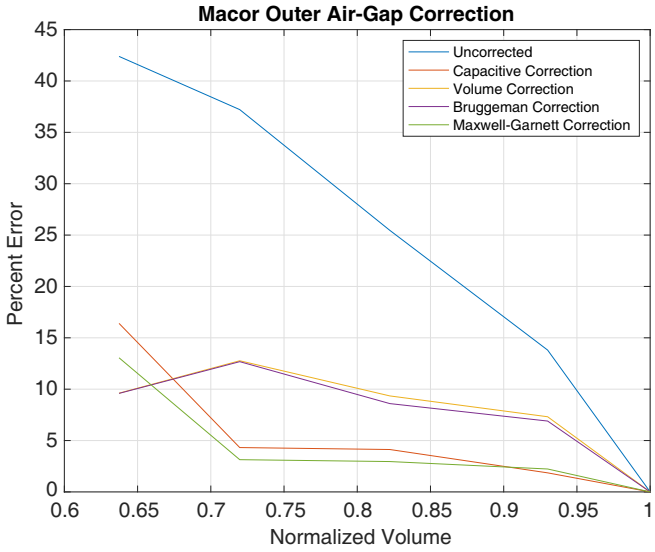

Figure 11. Percent error for outer air-gap correction methods for normalized volumes of Macor.

is shown for Eccosorb in Fig. 8, where percent error is given by $\% = |NG - AG|/NG * 100$, where NG and AG are the values measured at each field strength with No Gap and an Air Gap, respectively. The increased error in measured permittivity for inner air-gaps is shown for capacitive, volume, and Bruggeman air-gap correction approaches, and justifies the focus on outer air-gaps usage in testing. Additionally, the error across algorithms and air-gaps shows minimal variation to field strength for outer air-gaps, confirming this approach for measuring power dependent electronic properties of materials, as the approach does contribute power dependent variations. Each algorithm investigated is applied to the same set of measurements, decoupling the errors associated with alignment, air-gap, and MUT thickness measurements from each algorithm to recover the electronic properties of the MUT without an air-gap.

Results for materials tested and air-gap correction methods are shown in Figs. 9–11. The summary plot for HDPE, Fig. 9, demonstrates the capacitive correction method best reversed the error introduced by the air gap for all air-gaps tested, with the other correction methods failing to recover the permittivity to within %10 for any air-gap tested. Eccosorb, Fig. 10, demonstrates that all correction methods are able to recover the air-gap introduced error, but are limited by air-gaps of 0.52 mm for Capacitive and Bruggeman correction methods, and 0.84 mm for Maxwell-Garnett and Volume correction methods. Conversely, Macor, Fig. 11, demonstrates air-gap limits of 0.52 mm for Maxwell-Garnett and Volume correction methods, and 0.84 mm for Capacitive and Bruggeman correction methods.

7. CONCLUSION

A technique for measuring the microwave permittivity of conductive materials at high field strengths has been demonstrated by introducing an outer air-gap in a MUT. The effects introduced by the air-gap are reversed through air-gap correction algorithms. In comparison to permittivity measurements with no gap, permittivity measurements with an outer air-gap introduced less than 0.6 mm for the 7 mm coaxial air-line were able to recover measured permittivity with $\epsilon_r < \pm 0.2, 0.4$ and 0.5 for HDPE, Eccosorb, and Macor, respectively. The capacitive correction outperforms all other air-gap methodologies for low permittivity materials (HDPE $\epsilon_r = 2.4$, $\mu_r = 1$). Magnetic materials appear to have greater recovery of the correct permittivity and permeability for Bruggeman and simple volume correction as compared to that of the capacitive and Maxwell-Garnett approaches. Future work will focus on studying additional MUTs to develop trends in the optimal air-gap correction method.

ACKNOWLEDGMENT

This work was supported by the Office of Naval Research under N00014-16-1-2067.

REFERENCES

1. Nadaud, K., C. Borderon, R. Renoud, A. Ghalem, A. Crunteanu, L. Huitema, F. Dumas-Bouchiat, P. Marchet, C. Champeaux, and H. W. Gundel, "Domain wall motions in BST ferroelectric thin films in the microwave frequency range," *Appl. Phys. Lett.*, Vol. 109, No. 26, 1–5, 2016.
2. Borderon, C., R. Renoud, M. Ragheb, and H. W. Gundel, "Description of the low field nonlinear dielectric properties of ferroelectric and multiferroic materials," *Appl. Phys. Lett.*, Vol. 98, No. 11, 11–13, 2011.
3. Balci, O., E. O. Polat, N. Kakenov, and C. Kocabas, "Graphene-enabled electrically switchable radar-absorbing surfaces," *Nature Communications*, Vol. 6, 1–9, 2015.
4. Yao, X., X. Kou, and J. Qiu, "Multi-walled carbon nanotubes/polyaniline composites with negative permittivity and negative permeability," *Carbon*, Vol. 107, 261–267, 2016.
5. Che, R. C., C. Y. Zhi, C. Y. Liang, and X. G. Zhou, "Fabrication and microwave absorption of carbon nanotubes $CoFe_2O_4$ spinel nanocomposite," *Appl. Phys. Lett.*, Vol. 88, No. 3, 1–3, 2006.
6. Lv, R., F. Kang, J. Gu, X. Gui, J. Wei, K. Wang, and D. Wu, "Carbon nanotubes filled with ferromagnetic alloy nanowires: Lightweight and wide-band microwave absorber," *Appl. Phys. Lett.*, Vol. 93, No. 22, 2006–2009, 2008.
7. Zhang, B., J. Wang, J. Wang, S. Huo, B. Zhang, and Y. Tang, "Microwave absorption properties of lightweight absorber based on $Fe_{50}Ni_{50}$-coated poly(acrylonitrile) microspheres and reduced graphene oxide composites," *Journal of Magnetism and Magnetic Materials*, Vol. 413, 81–88, 2016.
8. Gui, X., W. Ye, J. Wei, K. Wang, R. Lv, H. Zhu, F. Kang, J. Gu, and D. Wu, "Optimization of electromagnetic matching of Fe-filled carbon nanotubes/ferrite composites for microwave absorption," *Journal of Physics D: Applied Physics*, Vol. 42, No. 7, 075002, 2009.
9. Ganchev, S. I., N. Qaddoumi, S. Bakhtiari, and R. Zoughi, "Calibration and measurement of dielectric properties of finite thickness composite sheets with open-ended coaxial sensors," *IEEE Transactions on Instrumentation and Measurement*, Vol. 44, No. 6, 1023–1029, 1995.
10. Drinovsky, J. and Z. Kejík, "Electromagnetic shielding efficiency measurement of composite materials," *Measurement Science Review*, Vol. 9, No. 4, 109–112, 2009.
11. Havrilla, M. J. and D. P. Nyquist, "Electromagnetic characterization of layered materials via direct and de-embed methods," *IEEE Transactions on Instrumentation and Measurement*, Vol. 55, No. 1, 158–163, 2006.
12. Paul, C. R., *Analysis of Multiconductor Transmission Lines*, Wiley-Interscience, 2008.
13. Nicolson, A. M. and G. F. Ross, "Measurement of the intrinsic properties of materials by time-domain techniques," *IEEE Transactions on Instrumentation and Measurement*, Vol. 19, No. 4, 377–382, 1970.
14. Weir, W. B., "Automatic measurement of complex dielectric constant and permeability at microwave frequencies," *Proceedings of the IEEE*, Vol. 62, No. 1, 33–36, 1974.
15. Baker-Jarvis, J., M. D. Janezic, J. H. Grosvenor, Jr., and R. G. Geyer, "Transmission/reflection and short-circuit line methods for measuring permittivity and permeability," *NASA STI/Recon Technical Report N*, Vol. 93, 12084, 1992.
16. Barry, W., "A broad-band, automated, stripline technique for the simultaneous measurement of complex permittivity and permeability," *IEEE Transactions on Microwave Theory and Techniques*, Vol. 34, No. 1, 80–84, 1986.
17. Hassan, A. M., J. Obrzut, and E. J. Garboczi, "A Q-band free-space characterization of carbon nanotube composites," *IEEE Transactions on Microwave Theory and Techniques*, Vol. 64, No. 11, 3807–3819, 2016.

18. Vanzura, E. J., J. R. Baker-Jarvis, J. H. Grosvenor, and M. D. Janezic, "Intercomparison of permittivity measurements using the transmission/reflection method in 7-mm coaxial transmission lines," *IEEE Transactions on Microwave Theory and Techniques*, Vol. 42, No. 11, 2063–2070, 1994.
19. Wang, Y., I. Hooper, E. Edwards, and P. S. Grant, "Gap-corrected thin-film permittivity and permeability measurement with a broadband coaxial line technique," *IEEE Transactions on Microwave Theory and Techniques*, Vol. 64, No. 3, 924–930, 2016.
20. Jamaian, S. S. and T. G. Mackay, "On limitations of the Bruggeman formalism for inverse homogenization," *Journal of Nanophotonics*, Vol. 4, No. 1, 1–8, 2010.
21. Baker-Jarvis, J., M. D. Janezic, J. H. Grosvenor, and R. G. Geyer, "Transmission/reflection and short-circuit line methods for measuring permittivity and permeability," Tech. Rep., NIST, 1992.
22. Whites, K. W., "Electromagnetic wave propagation through circular waveguides containing radially inhomogeneous lossy media," Tech. Rep., Construction Engineering Research Lab, (ARMY), Champaign, IL, 1989.
23. Fehlen, R. G., "Air gap error compensation for coaxial transmission line," Ph.D. dissertation, Air Force Institute, 2006.
24. Mattar, K. E., D. G. Watters, M. E. Brodwin, and L. S. Member, "Influence of wall contacts on measured complex permittivity spectra at coaxial line frequencies," *IEEE Transactions on Microwave Theory and Techniques*, Vol. 39, No. 3, 532–537, 1991.
25. Leuchtmann, P. and J. Rüfenacht, "On the calculation of the electrical properties of precision coaxial lines," *IEEE Transactions on Instrumentation and Measurement*, Vol. 53, No. 2, 392–397, 2004.
26. Kim, S., H. Wakatsuchi, J. J. Rushton, and D. F. Sievenpiper, "Switchable nonlinear metasurfaces for absorbing high power surface waves," *Applied Physics Letters*, Vol. 108, No. 4, 1–5, 2016.
27. Luo, Z., X. Chen, J. Long, R. Quarfoth, and D. Sievenpiper, "Nonlinear power-dependent impedance surface," *IEEE Transactions on Antennas and Propagation*, Vol. 63, No. 4, 1736–1745, 2015.
28. Riddle, B., J. Baker-Jarvis, and J. Krupka, "Complex permittivity measurements of common plastics over variable temperatures," *IEEE Transactions on Microwave Theory and Techniques*, Vol. 51, No. 3, 727–733, 2003.
29. Belous, A., O. Ovchar, and D. Mischuk, "Temperature trends of the permittivity in complex oxides of rare-earth elements with perovskite-type structure," *Condensed Matter Physics*, Vol. 6, No. 2, 251, 2003.